



Intrinsic Electron-Phonon Resistivity of Bi₂Se₃ in the Topological Regime

Dohun Kim,¹ Qiuzi Li,² Paul Syers,¹ Nicholas P. Butch,^{1,*} Johnpierre Paglione,¹ S. Das Sarma,^{1,2} and Michael S. Fuhrer^{1,†}

¹*Center for Nanophysics and Advanced Materials, Department of Physics,
University of Maryland, College Park, Maryland 20742-4111, USA*

²*Condensed Matter Theory Center, Department of Physics, University of Maryland,
College Park, Maryland 20742-4111, USA*

(Received 25 May 2012; published 15 October 2012)

We measure the temperature-dependent carrier density and resistivity of the topological surface state of thin exfoliated Bi₂Se₃ in the absence of bulk conduction. When the gate-tuned chemical potential is near or below the Dirac point, the carrier density is strongly temperature-dependent, reflecting thermal activation from the nearby bulk valence band, while, above the Dirac point, unipolar *n*-type surface conduction is observed with negligible thermal activation of bulk carriers. In this regime, linear resistivity vs temperature reflects intrinsic electron-acoustic phonon scattering. A quantitative comparison with a theoretical transport calculation including both phonon and disorder effects gives the ratio of deformation potential to Fermi velocity $D/\hbar v_F = 4.7 \text{ \AA}^{-1}$. This strong phonon scattering in the Bi₂Se₃ surface state gives intrinsic limits for the conductivity and charge carrier mobility at room temperature of $\sim 550 \mu\text{S}$ per surface and $\sim 10000 \text{ cm}^2/\text{V s}$.

DOI: [10.1103/PhysRevLett.109.166801](https://doi.org/10.1103/PhysRevLett.109.166801)

PACS numbers: 73.20.-r, 72.10.Di, 73.50.-h, 85.35.-p

The 3D topological insulators (TIs) have an insulating bulk but metallic surface states stemming from band inversion due to strong spin-orbit interaction [1,2]. The helicity of the surface carriers is protected by time-reversal symmetry and is exhibited in spin-momentum locking [3], which may be exploited in spintronic [4] and optospintronic devices [5], and the discovery of TI materials such as Bi₂Se₃ with a bulk band gap on the order of 300 meV [2] is anticipated to enable such topological electronic devices at room temperature. While the helical surface state is robust against backscattering by time-reversal-invariant disorder [6], the eventual surface conductivity and mobility are determined entirely by carrier scattering from disorder and phonons since scattering at angles less than π is possible in the two-dimensional surface state. The intrinsic limits to conductivity and mobility at finite temperature will be set by the electron-phonon interaction; hence, the study of electron-phonon coupling in TIs is of central importance in assessing potential electronic applications. The goal of the current work is to combine experiment and theory in order to ascertain the intrinsic limit to the 2D transport mobility of TI surface carriers arising from phonon scattering.

Experimental studies of inelastic scattering processes at the TI surface have been confined to angle-resolved photoemission [7,8] or helium atom surface scattering probes [9] of the quasiparticle or phonon lifetimes, respectively. These studies do not measure directly the resistivity, and the inferred electron-phonon coupling constants are not consistent with each other, varying by a factor of ≈ 5 . The high level of doping in bulk TI crystals, hence the dominant bulk conduction, hinders the unambiguous analysis of surface signatures in electronic transport [10,11]. However, we

recently demonstrated that, for Bi₂Se₃ thin ($\approx 10 \text{ nm}$) crystals with low bulk disorder, the top and bottom topological surface states are strongly electrostatically coupled and their Fermi energies are nearly identical and can be tuned together through the Dirac point by application of only a back gate voltage, allowing measurement of the carrier-density-dependent electronic transport properties of the topological surface states in the absence of a conducting bulk [12,13].

Here, we report the temperature (T) and gate-voltage (V_g) dependence of the longitudinal resistivity ρ_{xx} and Hall carrier density $n_H = 1/R_H e$ of the surface states of thin exfoliated Bi₂Se₃ crystals in the topological regime, where R_H is the Hall coefficient and e is the elemental charge. n_H is temperature-dependent for Fermi energies close to the bulk valence band and can be well described by thermal activation of carriers from a massive bulk band into the Dirac surface state. For a wide range of carrier densities ($2 \times 10^{12} \text{ cm}^{-2} < n_H < 8 \times 10^{12} \text{ cm}^{-2}$, spanning the majority of the range of *n*-type conduction), there is negligible activation of bulk carriers. There, we observe ρ_{xx} increasing linearly with temperature, with a slope at high carrier density $\approx 3 \Omega/\text{K}$. (For the purpose of comparison, this rate is more than an order of magnitude larger than the temperature dependence of the corresponding graphene resistivity [14,15].) Comparing with theoretical calculations, including the effect of disorder-induced charge fluctuations and temperature-dependent screening, we interpret the linear increase in resistivity as reflecting the electron-acoustic phonon scattering in the degenerate metallic surface state. For Fermi energies near the conduction band edge, we determine the ratio of deformation potential to Fermi velocity $D/\hbar v_F = 4.7 \text{ \AA}^{-1}$. For Fermi velocities

of $5\text{--}7 \times 10^5$ m/s as measured by angle-resolved photoemission (ARPES) at similar Fermi energies [16,17], the deformation potential is in the range 15–22 eV, in agreement with theoretical expectations.

Bi_2Se_3 devices were produced by the micromechanical cleavage of low-doped (carrier density $\sim 10^{17}$ cm $^{-3}$) bulk Bi_2Se_3 single crystals with bulk resistivity exceeding 2 m Ω cm at 300 K [10] on 300 nm SiO_2 /doped Si substrates, followed by patterning into Hall bar geometry with electron-beam lithography and Ar plasma etching. Au/Cr electrodes were defined by electron-beam lithography [see the inset of Fig. 1(b)]. A brief (≈ 10 s) selective surface treatment of the contact area with N_2 or Ar plasma before the deposition of metals was used to enhance Ohmic conduction of the contacts. To avoid band gap opening due to the hybridization of bottom and top surfaces [18,19], crystals with thickness of about 10 nm (confirmed by atomic force microscopy) were used in this study. In order to reduce high n -type doping commonly observed in microfabricated Bi_2Se_3 devices, we employed molecular charge transfer doping by thermal evaporation of 2,3,5,6-tetrafluoro-7,7,8,8-tetracyanoquinodimethane (F4TCNQ) organic molecules on the fabricated devices [12,20]. After F4TCNQ deposition, we typically measure n_{H} in the range $3\text{--}5 \times 10^{12}$ cm $^{-2}$ at zero gate voltage. The carrier density in the topological surface state at the bulk

conduction band edge is approximately 5×10^{12} cm $^{-2}$ per surface, or 1.0×10^{13} cm $^{-2}$ total for top and bottom surfaces; hence, the devices are in the topological regime before application of a back gate voltage. Temperature-dependent longitudinal and transverse resistivity were measured simultaneously, using two lock-in amplifiers and a commercial cryostat equipped with a 9 T superconducting magnet.

Figure 1(a) shows n_{H} as a function of gate voltage V_g and temperature T , where several line cuts with respect to V_g at various temperatures are plotted in Fig. 1(b). In general, we observe a gapless ambipolar electric field effect, which is indicated by the sign change in n_{H} at the charge neutrality point [$V_{g,0}$, dashed lines in Fig. 1(b)] associated with the Dirac point of the topological surface states. The positive (negative) divergence in n_{H} when approaching $V_{g,0}$ from above (below) is due to inhomogeneity-driven electron-hole puddles [12,21]. At low temperature (e.g., 2 K), $n_{\text{H}}(V_g)$ is linear over broad ranges of n and p doping with slope $dn_{\text{H}}/dV_g = C_g/e$, indicating a gate capacitance $C_g = 11$ nF cm $^{-2}$, as expected for 300 nm thick SiO_2 . However, as temperature is raised, $V_{g,0}$ shifts to more negative voltage and the slope dn_{H}/dV_g is reduced near and below $V_{g,0}$, while $n_{\text{H}}(V_g)$ remains temperature-independent for the unipolar n -type conduction regime ($V_g > -20$ V). The shift in $V_{g,0}$ shows thermally activated behavior with an activation energy of 60 meV, as determined from the Arrhenius fit of $V_{g,0}(T)$ in the range of $50 \text{ K} < T < 150 \text{ K}$.

We first explore the origin of the temperature dependence of n_{H} . In our previous study [12], we experimentally demonstrated by dual electrostatic gating that significant band bending is absent in thin (≈ 10 nm), lightly doped Bi_2Se_3 crystals due to strong capacitive coupling of the two topological surfaces through the high-dielectric-constant insulating bulk Bi_2Se_3 . Therefore, although a superficially similar shift of $V_{g,0}$ was observed in Ref. [22] and interpreted there as due to a reduction in the effective bulk gap due to band bending, we rule out this effect in our devices. Instead, we note that the energy scale for thermal activation corresponds well with the expected separation of the bulk valence band and the Dirac point of the topological surface band. Hence, significant thermal activation of electrons from the bulk valence band to the surface band, hence leaving holes in the bulk valence band, should occur at modest temperatures, resulting in a negative shift of $V_{g,0}$.

We develop a more detailed model of $n_{\text{H}}(T)$ as follows. We assume that n_{H} reflects the density of surface carriers only. Since in a multiband system the net Hall conductivity is the mobility-weighted average of the Hall conductivities of each band, the assumption reflects the expectation of much lower carrier mobility for the bulk valence band, which has much higher effective mass and no topological protection from backscattering. We assume that two bands

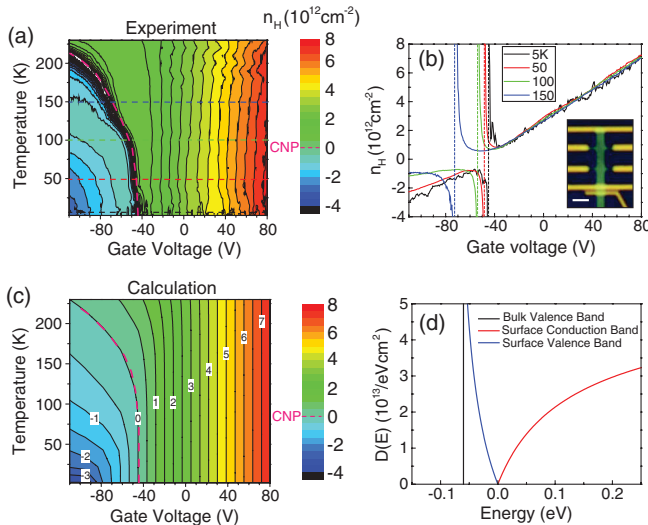


FIG. 1 (color). (a) Measured Hall carrier density (n_{H}) of a thin exfoliated Bi_2Se_3 device as a function of back gate voltage (V_g) and temperature (T). The pink dashed curve shows a T -dependent trace of a charge neutrality point (CNP; $V_{g,0}$) (b) n_{H} vs V_g at various temperatures indicated by dashed lines in (a). Dashed lines indicate points of charge neutrality. The inset shows an optical micrograph of the device. The scale bar is 2 μm . (c) Calculated surface band carrier density as a function of V_g and T using a thermal activation model discussed in the text. (d) Energy-dependent density of states $D(E)$ for the thermal activation model, showing surface (red and blue solid lines) bands and a bulk valence (black solid line) band.

are important in determining $n_H(T)$: the surface band with dispersion $E_{2D}(k) = \hbar v_{F,0}k + \frac{\hbar^2 k^2}{2m_s^*}$ and the bulk valence band with dispersion $E_{3D}(k) = E_v - \frac{\hbar^2 k^2}{2m_b^*}$, where we estimate the energy of the band edge $E_v = -60$ meV from the observed temperature-dependent shift of $V_{g,0}$. For the calculation, we used the parameters of the Fermi velocity near the Dirac point $v_{F,0} = 3 \times 10^7$ cm/s, and the effective mass $m_s^* = 0.3m_e$ of the surface band and the effective mass $m_b^* = 2.6m_e$ of the bulk valence band, which are reasonable for Bi_2Se_3 from the ARPES measurements [16,17,23].

Figure 1(d) shows the Bi_2Se_3 density of states $D(E)$ used in our model. Figure 1(c) shows the calculated $n_H(V_g, T)$ based on $D(E)$. The model captures the essential characteristics of the measured $n_H(V_g, T)$ [Fig. 1(a)]: $V_{g,0}$ shifts to negative voltage in a thermally activated manner; C_g in the hole-doped region is comparable to that of 300 nm SiO_2 at low temperatures but is gradually suppressed as temperature is increased due to thermal activation from bulk valence band; and n_H in the electron-doped region ($V_g > -20$ V) is nearly independent of temperature. The model fails to describe the divergence of n_H near $V_{g,0}$ due to charge inhomogeneity, which is not included in the model. However, the overall success of the model supports our picture of unipolar n -type transport dominated by the topological surface state in the absence of bulk carriers in the region $-20 \text{ V} < V_g < 80 \text{ V}$, corresponding to carrier densities in the topological surface of $1.5\text{--}8 \times 10^{12} \text{ cm}^{-2}$.

We now discuss temperature-dependent longitudinal resistivity $\rho_{xx}(T)$ in the unipolar n -type regime. Figure 2(a) shows $\rho_{xx}(T)$ of device 1 at different n_H tuned by V_g . Generally, $\rho_{xx}(T)$ is metallic ($d\rho_{xx}/dT > 0$) and saturates at low $T < 40$ K, as expected for gapless surface states. In the intermediate temperatures of $50 \text{ K} < T < 150 \text{ K}$, $\rho_{xx}(T)$ is linearly increasing with T , consistent with scattering of degenerate electrons with phonons that are populated according to the classical equipartition distribution.

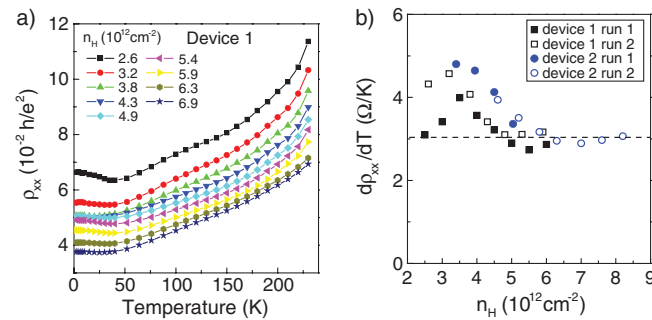


FIG. 2 (color). (a) Longitudinal resistivity ρ_{xx} of device 1 as a function of temperature at different carrier densities tuned by the back gate. (b) Slope of ρ_{xx} vs carrier density in the linear temperature regime ($50 \text{ K} < T < 150 \text{ K}$). The dashed line indicates the high carrier-density value of the slope used to compare to the theoretical model.

For device 1, the highest Hall mobility at low temperature is $1430 \text{ cm}^2/\text{Vs}$ at $n_H = 2.6 \times 10^{12} \text{ cm}^{-2}$, which is reduced by more than 20% to $1120 \text{ cm}^2/\text{Vs}$ at $T = 150 \text{ K}$. Figure 2(b) shows the average slope $d\rho_{xx}/dT$ for $50 \text{ K} < T < 150 \text{ K}$ at different n_H for two different experimental runs with two different samples. $d\rho_{xx}/dT$ varies by less than a factor of 1.75, while the carrier density varies almost fourfold. A broad peak in $d\rho_{xx}/dT$ occurs around $n_H = 3.5 \times 10^{12} \text{ cm}^{-2}$, and $d\rho_{xx}/dT$ approaches a roughly density-independent value of $\approx 3 \text{ } \Omega/\text{K}$ at high n_H .

In the high-temperature and high carrier-density regimes, the temperature dependence of resistivity $d\rho_{xx}/dT$ mainly comes from the electron-phonon scattering, the asymptotic high-temperature behavior of which can be expressed as

$$\rho_{\text{ph}} \sim \frac{\pi D^2 k_B T}{e^2 \hbar v_F^2 \nu_{\text{ph}}^2 \rho_m}, \quad (1)$$

where ρ_{ph} is the electron-phonon scattering limited resistivity, D is the deformation potential, and $\nu_{\text{ph}} = 2900 \text{ m/s}$ is the phonon velocity. $\rho_m = 7.68 \times 10^{-7} \text{ g/cm}^2$ is the mass density of Bi_2Se_3 for a single quintuple layer (thickness $\sim 1 \text{ nm}$) corresponding to the penetration length of the topological surface state into the bulk [24]. As can be seen from Eq. (1), $d\rho_{\text{ph}}/dT$ is determined by the ratio of the deformation potential to the Fermi velocity $D/\hbar v_F$.

In real samples with disorder, other effects (e.g., screening, potential fluctuation-induced puddles) may contribute to the temperature dependence of the resistivity. Charged impurity scattering and potential fluctuations play important roles in determining the minimum conductivity and low-temperature transport of the topological surface state [12,13,25]. Because of the strong suppression of the back-scattering in TI surface transport, metallic temperature-dependent screening effects are relatively weak [26] and are therefore not discussed here. Thermal activation across potential fluctuations gives rise to an insulating behavior of temperature-dependent resistivity ($d\rho/dT < 0$), which may be important at low carrier density where phonon effects are suppressed. To determine whether Eq. (1) accurately describes the resistivity in our samples, we have developed a realistic model of temperature-dependent resistivity of the topological surface state, including electron-phonon scattering [14,27] and the effects of charged impurity scattering [26] and potential fluctuations [12,21]. We have calculated the resistivity by using Boltzmann transport theory and effective medium theory, in which we assume the potential fluctuation follows a Gaussian form parametrized by the potential strength s . The detailed theories have been presented elsewhere [25,26].

One serious issue in a quantitative theoretical determination of the temperature dependence is that the deformation potential coupling for the surface electrons is simply not known, and theoretical determination from first principles is imprecise. Since the resistivity depends on the square of the deformation potential $\rho \sim D^2$, any imprecision in D is magnified in ρ . An

experiment-theory comparison is therefore essential to determine the value of D . We have therefore carried out a careful regression fit to make the linear T dependence of the experiment and theory agree with each other, so as to obtain the best possible estimate of D in the system.

Figures 3(a) and 3(b) show the calculated $\rho_{xx}(T)$ for two different disorder strengths in the range of temperatures for which the experiment sees linear $\rho_{xx}(T)$. We find the best match to the experimentally measured $d\rho_{xx}/dT$ at high carrier density for a deformation potential $D = 22$ eV and Fermi velocity $v_F = 7 \times 10^5$ m/s ($D/\hbar v_F = 4.7 \text{ \AA}^{-1}$). We take the effective background dielectric constant to be $\kappa = 33$, the average distance of the charged impurity from the topological surface $d = 1 \text{ \AA}$. In Fig. 3(a), the charged impurity density $n_{\text{imp}} = 3 \times 10^{13} \text{ cm}^{-2}$ (charge inhomogeneity-driven potential fluctuation $s = 90$ meV), and in Fig. 3(b) $n_{\text{imp}} = 1.5 \times 10^{13} \text{ cm}^{-2}$ ($s = 65$ meV). The disorder strength is the major determinant of the carrier-density dependence of the resistivity, as reflected in Figs. 3(a) and 3(b). The calculated resistivities bracket the experimental data, indicating that the experimental disorder is comparable to the estimates. A quantitative agreement in the carrier-density dependence of the resistivity is not expected since the model does not include the significant nonlinearity of the surface bands [13].

Figure 3(c) shows the calculated slope $d\rho_{xx}/dT$ for $50 \text{ K} < T < 150 \text{ K}$ as a function of carrier density n . At low n , the slope increases monotonically with density and is disorder-dependent. At high n , the slope asymptotically approaches a constant consistent with Eq. (1). The results indicate that the slope measured at high n reflects electron-phonon scattering even at large disorder strength; hence, the experimentally measured slope of 3 \Omega/K determines

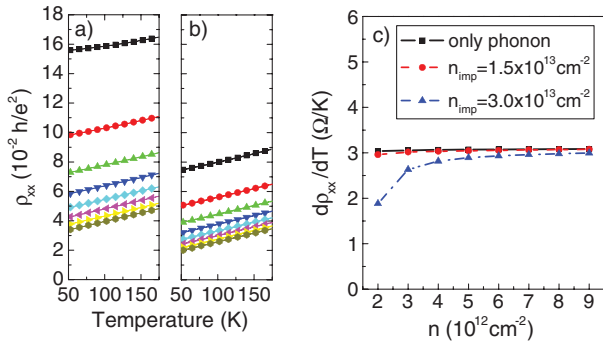


FIG. 3 (color). (a),(b) Calculated total resistivity ρ_{xx} as a function of temperature for different carrier densities $n = 2, 3, 4, 5, 6, 7, 8, 9 \times 10^{12} \text{ cm}^{-2}$ from top to bottom. In (a), the charged impurity density is $n_{\text{imp}} = 3 \times 10^{13} \text{ cm}^{-2}$, and the potential fluctuation strength is $s = 90$ meV. In (b), $n_{\text{imp}} = 1.5 \times 10^{13} \text{ cm}^{-2}$ and $s = 65$ meV. (c) Calculated slope $d\rho_{xx}/dT$ vs n in the linear temperature regime ($50 \text{ K} < T < 150 \text{ K}$). The solid line is the result including only electron-phonon scattering, while the dot-dashed and dashed lines correspond to Figs. 3(a) and 3(b), respectively.

the ratio $D/\hbar v_F = 4.7 \text{ \AA}^{-1}$ at high carrier density. Assuming a Fermi velocity $v_F = 5\text{--}7 \times 10^5$ m/s consistent with ARPES measurements [16,17,23], the corresponding deformation potential is $D = 15\text{--}22$ eV. The experimentally observed $d\rho_{xx}/dT$ shows a peak at lower carrier density, which we understand as a competition between decreasing v_F due to the nonlinearity of the surface bands (not included in the theory), which leads to increased $d\rho_{xx}/dT$, and thermal activation across the potential fluctuations, which leads to a reduced $d\rho_{xx}/dT$ near the Dirac point, as seen in Fig. 3(c).

In contrast to the intermediate- T behavior, the resistivity at higher $T > 150$ K is highly nonlinear in T and becomes significantly dependent on n_H , increasing for decreasing n_H [Fig. 2(a)]. Similar behavior was observed in graphene [15], where the nonlinear $\rho_{xx}(T)$ was attributed to remote interfacial scattering of electrons with polar optical phonons in the SiO_2 substrate. However, fitting high-temperature resistivity of Bi_2Se_3 devices to the activated form $\rho_{xx}(T) = \rho_0 e^{-\Delta E/k_B T}$ yields $130 \text{ meV} < \Delta E < 170 \text{ meV}$, depending on n_H , which appears unreasonable for optical phonons of the substrate or Bi_2Se_3 . Moreover, we find that the resistivity between $250 \text{ K} < T < 300 \text{ K}$ shows appreciable hysteresis in temperature, which is likely associated with charge transfer from SiO_2 substrates to the bottom surface or absorption and desorption of F4TCNQ molecules on the top surface of the device. Thus, we ascribe the observed nonlinear behavior at $T > 200$ K to an extrinsic contribution to $\rho_{xx}(T)$, whose origin is not yet understood.

In conclusion, we have studied temperature-dependent electronic transport in the topological surface states of Bi_2Se_3 . We find significant activation of carriers from the bulk valence band for Fermi energies near or below the Dirac point but identify a region of unipolar electron conduction where activation of bulk carriers is negligible. In this regime, the temperature dependence of the resistivity $d\rho_{xx}/dT$ is relatively independent of carrier density and is used to extract a ratio of deformation potential to Fermi velocity $D/\hbar v_F = 4.7 \text{ \AA}^{-1}$, which gauges the strength of the intrinsic electron-acoustic phonon interaction in Bi_2Se_3 . The strong acoustic phonon scattering places an intrinsic limit on the conductivity of the Bi_2Se_3 surface states of $\sim 550 \text{ \mu S} = 14e^2/h$ per surface, approximately 60 times lower than graphene's intrinsic conductivity at room temperature. The intrinsic mobility limited by electron-acoustic phonon scattering will be carrier-density-dependent and highest at low carrier density. Assuming a factor of 2 reduction in v_F at the Dirac point ($\sim 3 \times 10^7$ cm/s) compared to near the bulk conduction band edge ($\sim 5\text{--}7 \times 10^7$ cm/s), the intrinsic carrier density at room temperature is $\sim 2 \times 10^{11} \text{ cm}^{-2}$ and the highest achievable room temperature mobility is $< 10,000 \text{ cm}^2/\text{Vs}$. Our combined theoretical-experimental work also provides an accurate estimate for the deformation potential coupling in the Bi_2Se_3 surface carriers to be $15\text{--}22$ eV.

The authors acknowledge useful conversations with E. H. Hwang, S. Adam, and S. Giraud. This work was supported by NSF Grant No. DMR-11-05224, DARPA QuEST, and Microsoft Q.

*Present address: Condensed Matter and Materials Division, Lawrence Livermore National Laboratory, Livermore, CA 94550, USA.

†mfuhrer@umd.edu

- [1] L. Fu, C. L. Kane, and E. J. Mele, *Phys. Rev. Lett.* **98**, 106803 (2007).
- [2] H. J. Zhang, C. X. Liu, X. L. Qi, X. Dai, Z. Fang, and S. C. Zhang, *Nature Phys.* **5**, 438 (2009).
- [3] D. Hsieh *et al.*, *Science* **323**, 919 (2009).
- [4] I. Appelbaum, H. D. Drew, and M. S. Fuhrer, *Appl. Phys. Lett.* **98**, 023103 (2011).
- [5] J. W. McIver, D. Hsieh, H. Steinberg, P. Jarillo-Herrero, and N. Gedik, *Nature Nanotech.* **7**, 96 (2012).
- [6] C. L. Kane and E. J. Mele, *Phys. Rev. Lett.* **95**, 226801 (2005).
- [7] R. C. Hatch, M. Bianchi, D. D. Guan, S. N. Bao, J. L. Mi, B. B. Iversen, L. Nilsson, L. Hornekær, and P. Hofmann, *Phys. Rev. B* **83**, 241303 (2011).
- [8] Z.-H. Pan, A. V. Fedorov, D. Gardner, Y. S. Lee, S. Chu, and T. Valla, *Phys. Rev. Lett.* **108**, 187001 (2012).
- [9] X. T. Zhu, L. Santos, C. Howard, R. Sankar, F. C. Chou, C. Chamon, and M. El-Batanouny, *Phys. Rev. Lett.* **108**, 185501 (2012).
- [10] N. P. Butch, K. Kirshenbaum, P. Syers, A. B. Sushkov, G. S. Jenkins, H. D. Drew, and J. Paglione, *Phys. Rev. B* **81**, 241301 (2010).
- [11] H. Steinberg, D. R. Gardner, Y. S. Lee, and P. Jarillo-Herrero, *Nano Lett.* **10**, 5032 (2010).
- [12] D. Kim, S. Cho, N. P. Butch, P. Syers, K. Kirshenbaum, S. Adam, J. Paglione, and M. S. Fuhrer, *Nature Phys.* **8**, 460 (2012).
- [13] S. Adam, E. H. Hwang, and S. Das Sarma, *Phys. Rev. B* **85**, 235413 (2012); see also D. Culcer, E. H. Hwang, T. D. Stanescu, and S. Das Sarma, *ibid.* **82**, 155457 (2010).
- [14] E. H. Hwang and S. Das Sarma, *Phys. Rev. B* **77**, 115449 (2008).
- [15] J. H. Chen, C. Jang, S. Xiao, M. Ishigami, and M. S. Fuhrer, *Nature Nanotech.* **3**, 206 (2008).
- [16] K. Kuroda *et al.*, *Phys. Rev. Lett.* **105**, 076802 (2010).
- [17] Z. H. Zhu *et al.*, *Phys. Rev. Lett.* **107**, 186405 (2011).
- [18] S. Cho, N. P. Butch, J. Paglione, and M. S. Fuhrer, *Nano Lett.* **11**, 1925 (2011).
- [19] Y. Zhang *et al.*, *Nature Phys.* **6**, 584 (2010).
- [20] C. Coletti, C. Riedl, D. S. Lee, B. Krauss, L. Patthey, K. von Klitzing, J. H. Smet, and U. Starke, *Phys. Rev. B* **81**, 235401 (2010).
- [21] H. Beidenkopf, P. Roushan, J. Seo, L. Gorman, I. Drozdov, Y. S. Hor, R. J. Cava, and A. Yazdani, *Nature Phys.* **7**, 939 (2011).
- [22] J. G. Checkelsky, Y. S. Hor, R. J. Cava, and N. P. Ong, *Phys. Rev. Lett.* **106**, 196801 (2011).
- [23] Y. Xia *et al.*, *Nature Phys.* **5**, 398 (2009).
- [24] C. X. Liu, X. L. Qi, H. J. Zhang, X. Dai, Z. Fang, and S. C. Zhang, *Phys. Rev. B* **82**, 045122 (2010).
- [25] Q. Li, E. Rossi, and S. Das Sarma (unpublished).
- [26] Q. Li, E. H. Hwang, and S. Das Sarma, *Phys. Rev. B* **84**, 115442 (2011).
- [27] S. Giraud and R. Egger, *Phys. Rev. B* **83**, 245322 (2011); S. Giraud, A. Kundu, and R. Egger, *ibid.* **85**, 035441 (2012).